UDC 621.313.332 https://doi.org/10.20998/2074-272X.2024.2.10

L.I. Mazurenko, O.V. Dzhura, M.O. Shykhnenko

Steady-state analysis of a hybrid power supply system using an induction generator with a shunt AC/DC converter

Hybrid power supply systems (HPSSs) are considered as a good option for electric power supply of remotely located from the grid consumers due to significant fuel savings compared to diesel sets. Quick development and improvement of HPSSs may be achieved using specialized methodologies and programs. In the paper a schematic diagram is proposed and operation principles of a 400 V / 50 Hz HPSS were developed. The system's main component is the master generating unit of the hydropower plant using a 250 kW induction generator (IG). The voltage of the system is controlled by the controller of the AC/DC power converter. The electrical frequency of the system is controlled by the speed controller of the hydropower turbine. A wind turbine, an energy storage system and a regulated dump load are connected to the IG through the AC/DC converter. ***Goal.*** *The paper aims to develop a methodology for steady state performance analysis of the hydraulic turbine driven isolated IG operating in parallel through an AC/DC power converter with additional sources and consumers of active power.* ***Methodology.*** *The methodology for evaluation of performance characteristics of the IG operating in the proposed system has been developed. The methodology is based on the equivalent circuit of the system, equations of active and reactive power balance in the system and the superposition method.* ***Results.*** *The equations of frequency, voltage and power regulators of the system are given. The performance characteristics of the IG operating in the system supplying resistive and RL load in «constant voltage – constant frequency» mode are obtained.* ***Novelty.*** *The developed methodology is innovative in taking into account the control algorithms of the system. The comparative analysis of the IG's performance operating in the stand-alone generating unit and in the generating unit connected to the proposed system is performed.* ***Practical value.*** *The developed methodology can be used for development and performance improvement of hybrid AC power systems.* References 19, table 1, figures 4.
Key words: **hybrid power system, induction generator, superposition method, equivalent circuit.**

Гібридні системи електропостачання (ГСЕ) розглядаються як хороший варіант для електропостачання віддалених від мережі споживачів завдяки значній економії палива порівняно з дизель-агрегатами. Швидка розробка і вдосконалення ГСЕ можуть бути досягнуті за допомогою спеціалізованих методик і програм. В статті запропоновано схемне рішення та розроблено принципи роботи ГСЕ промислової напруги і частоти 400 В / 50 Гц. Система побудована на основі ведучого гідроелектроагрегата з асинхронним генератором (АГ) потужністю 250 кВт. Стабілізація напруги системи забезпечується силовим AC/DC перетворювачем, а стабілізація електричної частоти системи – регулятором частоти обертання гідротурбіни. Вітроустановка, накопичувач енергії і регульоване баластне навантаження підключаються до АГ через AC/DC перетворювач. ***Метою*** *роботи є розробка методики розрахунку характеристик автономного АГ з гідротурбінним приводом, що працює паралельно через AC/DC перетворювач з додатковими джерелами та споживачами активної потужності. Розроблено* ***методику*** *розрахунку характеристик АГ запропонованої системи. Розроблена методика базується на основі еквівалентної схеми заміщення системи, рівнянь балансу активної і реактивної потужності та методу накладання. Наведено рівняння регуляторів частоти, напруги і потужності системи. З допомогою розробленої методики виконано розрахунки характеристик АГ за активного і активно-індуктивного навантаження споживачів при умові підтримання постійного значення напруги АГ і електричної частоти в системі. Створена методика має* ***новизну*** *в частині врахування алгоритмів керування системою. Проведено аналіз і співставлення характеристик АГ отриманих за його роботи в складі гідроелектроагрегата працюючого автономно і в складі запропонованої системи.* ***Отримані результати*** *можуть бути використані при розробці та для покращення технічних характеристик гібридних систем електропостачання змінного струму.* Бібл. 19, табл. 1, рис. 4.
Ключові слова: **гібридна система електропостачання, асинхронний генератор, метод накладання, схема заміщення.**

Introduction. Isolated power supply systems and modern distributed generation systems are capable to operate off-grid thus ensuring elimination of interruptions in power supply during grid outages and blackouts. These systems can reduce the cost of construction and losses of both power transmission and distribution lines caused by power transmission to local consumers located remotely from power transmission lines [1-4]. Photovoltaic systems, wind turbines (WTs), hydropower turbine equipped generating units (HTGUs), geothermal power plants, etc. are often combined with each other in distributed generation and isolated power supply systems to improve their performance. Electric power generating systems using different renewable primary energy sources are called hybrid power supply systems (HPSSs). When necessarily to provide a more reliable power supply, diesel power sets may be integrated in the HPSSs.

Today's power ratings of HTGUs, WTs and diesel power sets used in HPSSs are generally in the range 3-4 MW. WTs and HTGUs of this power range may be designed using permanent magnet generators, synchronous generators, doubly-fed and squirrel cage IGs [5-7]. The efficiencies of permanent magnet generators and synchronous generators are somewhat higher comparing to IGs, but IGs are simpler to service and repair. Moreover, due to lower price and lower maintenance costs, IGs are paid off sooner.

The solution of problems related to the performance analysis and evaluation of indicators of efficiency of energy conversion of IGs driven by regulated prime movers, such as hydraulic turbines (HTs) and diesel engines (DEs), has been successfully carried out and reported in the literature [8-10]. At the same time it should be noted, that methodologies developed for the steady-state analysis of stand-alone IGs using IG equivalent circuit are not adapted for performance analysis of IGs operating in parallel with various electric power sources within off-grid HPSSs. The study of the performance characteristics of IGs interconnected to electromechanical systems is a more complex objective requiring the development of complex mathematical

models [11, 12]. Complex dynamic models are a powerful tool for scientific investigations but they require a lot of computational efforts and time for debugging. Therefore, development of static mathematical models and new universal methodologies suitable for performing such studies or revision of existing ones is up to date.

The purpose of the article is to develop and test a methodology for steady state performance analysis of the induction generator driven by a hydraulic turbine of the master hydropower turbine equipped generating unit and operating in «constant voltage – constant frequency» mode in parallel through an electronic AC/DC power converter with sources and consumers of active power in the hydro-wind-battery hybrid power supply system supplying a three phase load.

Configuration and operating principles of the HPSS. The proposed HPSS (Fig. 1) consist of a master-HTGU with IG, a variable speed WT, an energy storage system (ESS) and a regulated dump load (RDL). The G2 generator of the WT is connected to the IG G1 through AC/DC voltage source converters VSC1 and VSC2. Both RDL and ESS are connected to the IG G1 through the VSC1. Power VSCs allow performing smooth power control of the sources of electric energy [13, 14]. The ESS can be of different types: flywheel ESS, battery ESS, supercapacitor based, etc. [15, 16]. The HPSS of Fig. 1 can operate both on-grid and off-grid. The HTGU consists of the IG G1, a regulated HT, the VSC1 converter and a bank of compensation capacitors (BCC) for self-excitation of the IG when the HPSS is off-grid. If hydro energy is unavailable in the region, diesel engines (DEs) may be used instead of HTs. Regulation of the electrical frequency in the system is carried out by the speed controller of the HT or DE. The controller of the WT uses wind speed and rotational speed of the WT for output power control of the wind generator. The ESS is provided to reduce frequency overshoot in transient modes and to limit the active power of the IG G1 during short-term peak demand. The RDL is intended mainly to consume active power excess in the system when the ESS is fully charged. It can also be used for «frequency-responsive» spinning reserve regulation [17, 18].

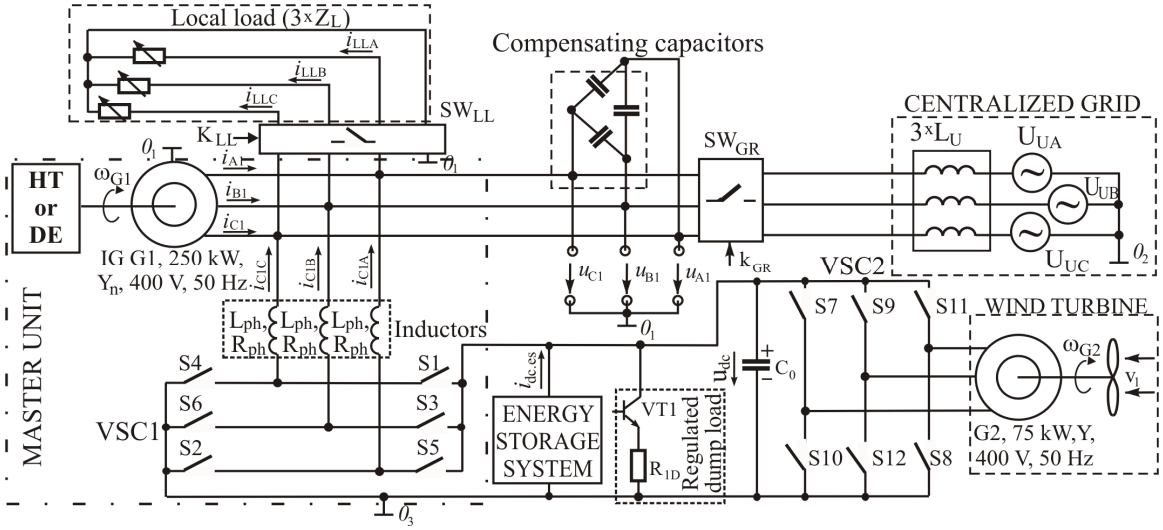

Fig. 1. Schematic diagram of the hybrid power supply system

Equations of frequency, voltage and power controllers are as follows.

- AC voltage, DC voltage and HTGU speed controllers

$$U_g^* = \text{const}; \quad (1)$$

$$U_{dc}^* = \text{const}; \quad (2)$$

$$\omega_e^* = \text{const}. \quad (3)$$

- RDL controller

$$P_{DL}^* = P_{EX}^* + \Delta P_{DL}^*, \quad (4)$$

where

$$\Delta P_{DL}^* = \begin{cases} -\Delta P_{EL}^*, \ \Delta P_{EL}^* < 0 \text{ and } \omega_{\min}^* < \omega_e < \omega_{\max}^*; \\ \Delta P_{DL1}^*, \text{ ESS is charged and } \omega_e > \omega_{\max}^*; \\ \Delta P_{DL2}^*, \text{ ESS is discharged and } \omega_e < \omega_{\min}^*; \\ 0, \text{ else}; \end{cases}$$

$$\Delta P_{EL}^* = P_L + P_{EX}^* - P_{WG} - P_{ES};$$

$$\Delta P_{DL1}^* = \max\left(0, \tilde{\omega}_{\max} k_{p1} + \int \tilde{\omega}_{\max} k_{i1}\right);$$

$$\Delta P_{DL2}^* = \max\left(-P_{EX}^*, \tilde{\omega}_{\min} k_{p1} + \int \tilde{\omega}_{\min} k_{i1}\right);$$

$$\tilde{\omega}_{\min} = \omega_e - \left(\omega_{\min}^* + \omega_h^*\right), \ \tilde{\omega}_{\max} = \omega_e - \left(\omega_{\max}^* - \omega_h^*\right).$$

- ESS controller

$$P_{ES}^* = \begin{cases} P_{ES1}^*, \text{ ESS is charged and } \omega_e > \omega_{\min}^*; \\ P_{ES2}^*, \text{ ESS is charged and } \omega_e < \omega_{\min}^*; \\ P_{ES3}^*, \text{ ESS is discharged, } \omega_e > \omega_{\min}^* \\ \quad \text{and } I_g < k_{gI} I_{gN}; \\ P_{ES4}^*, \text{ ESS is discharged and } \omega_e > \omega_{\max}^*; \\ 0, \text{ else}, \end{cases} \quad (5)$$

where

$$P_{ES1}^* = \max\left(0, \tilde{I}_{g.\max} k_{p2} + \int \tilde{I}_{g.\max} k_{i2}\right);$$

$$P_{ES2}^* = \max\left(0, -\tilde{\omega}_{\min} k_{p2} - \int \tilde{\omega}_{\min} k_{i2}\right);$$

$$P_{ES3}^* = -I_{dc.es}^* U_{dc};$$

$$P_{ES4}^* = \min\left(0, -\tilde{\omega}_{\max} k_{p2} - \int \tilde{\omega}_{\max} k_{i2}\right);$$

$$\tilde{I}_{g.\max} = I_g - I_{g.\max}^*.$$

The WT speed control is described in [17].

In the above equations U_g^* is the RMS reference value of phase voltage of the IG; ω_e^* is the angular electrical frequency reference in the system; U_{dc}^* is the DC-side voltage reference of the VSC1; P_{EX}^* is the «frequency-responsive» spinning reserve reference regulated with the RDL controller; P_L – is the active power demand; P_{WG} is the output active power of the WT; P_{ES}^* is the output power of the ESS assumed to be of positive sign while discharging of the ESS; P_{DL}^* is the active power reference of the RDL; I_g, $I_{g.\max}^*$, I_{gN} are values of actual, maximum reference and nominal RMS phase current of the IG; k_{p1}, k_{i1}, k_{p2}, k_{i2}, k_{gI} are positive constants; $\omega_{\max}^*$, $\omega_{\min}^*$, ω_e are values of maximum frequency reference, minimum frequency reference and actual angular electrical frequency in the system; $0 < \omega_h^* << \left(\omega_{\max}^* - \omega_{\min}^*\right) \cdot 0{,}5$; $I_{dc.es}^*$ is the input current reference of the ESS.

It is clear from (4), that when the sum of the active power demand of the local load and spinning reserve reference $P_L + P_{EX}^*$ is greater than the total output power of the WT and ESS and $\omega_{\min}^* < \omega_e < \omega_{\max}^*$, then $P_{DL} = P_{EX}^*$. When $P_{EX}^* < P_{WG} + P_{ES} - P_L$, we have an excess of active power in the system. In this case, if $\omega_{\min}^* < \omega_e < \omega_{\max}^*$, the power of the RDL is equal to $P_{DL}^* = P_{WG} + P_{ES} - P_L$ and the output active power of the IG is zero. If the electrical frequency in the system exceeds $\left(\omega_{\min}^* ... \omega_{\max}^*\right)$ limits and with current state of charge the ESS cannot perform frequency regulation, then the RDL performs this objective within the limits of its functional capabilities.

When the ESS is charged, as can be seen from (5), if $\omega_{\min}^* < \omega_e$, the ESS controller limits the current value of the generator to the $I_{g.\max}^*$ value level or, if the ω_e value falls below $\omega_{\min}^*$, it adjusts the ω_e value to the $\omega_{\min}^* + \omega_h^*$ level. At the same time, in accordance with (3), the frequency of the HPSS of Fig. 1 is regulated by the speed controller of the HTGU.

When the ESS is discharged and the output active power of the IG is sufficiently lower than its rated output and $\omega_{\min}^* < \omega_e$, then the ESS is being charged. At the same time, the value of the ESS power consumed is regulated by adjusting the value of the current $I_{dc.es}^*$. If there is a frequency error such that $\omega_e > \omega_{\max}^*$, and the ESS is discharged, then the controller of the ESS adjusts the ω_e value to the $\omega_{\max}^* - \omega_h^*$ level.

The methodology for performance analysis of the IG operating in the HPSS. To obtain performance characteristics of the HPSS, we will use shown in Fig. 2 proposed equivalent circuit (EC) of the system where all components of the system of Fig. 1 are represented by equivalent impedances.

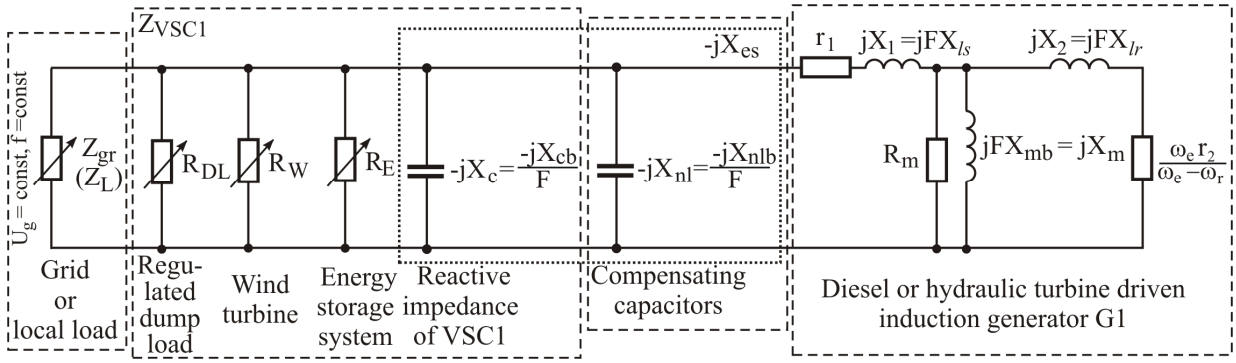

Fig. 2. Equivalent circuit of the hybrid power supply system

In Fig. 2 r_1, r_2, X_1, X_2 are the stator and rotor resistance and leakage reactance; ω_r is the electrical angular speed of the rotor of the IG; R_m is the core loss resistance; $F = \omega_e/\omega_{eN}$ is the per unit stator frequency of the IG; ω_{eN} is the nominal angular frequency of the stator; X_m is the magnetizing reactance; R_{DL}, R_W, R_E are equivalent resistances of RDL, WT and ESS. The values of reactances X_{ls}, X_{lr}, X_{cb}, X_{nlb}, X_{mb} refer to the base (rated) frequency of 50 Hz.

If we assume U_g = const and ω_e = const the EC of Fig. 2 can be used for performance analysis of the IG operating both in the off-grid HPSS supplying local load with Z_L impedance and on-grid with Z_{gr} input impedance of the grid.

To maintain the balance between power supply and demand for active and reactive power in the EC of Fig. 2, both real and imaginary part of the sum of admittances Y_S, Y_m and Y_R must be zero

$$\mathrm{Re}\left(Y_S + Y_m + Y_R\right) = 0; \quad (6)$$

$$\mathrm{Im}\left(Y_S + Y_m + Y_R\right) = 0, \quad (7)$$

where

$$Y_S = \left(r_1 + jX_1 - \frac{jX_{es}Z_{eq}}{Z_{eq} - jX_{es}} \right)^{-1};$$

$$Y_m = \frac{1}{jX_m} + \frac{1}{R_m}; \quad Y_R = \frac{1}{jX_2 + r_2/s};$$

$$X_{es} = X_c + X_{nl}; \quad Z_L = R_L + jX_L = z_l e^{j\varphi_L};$$

$$Z_{eq} = 1/\left(\left(Z_L\right)^{-1} + \left(R_{DL}\right)^{-1} + \left(R_W\right)^{-1} + \left(R_E\right)^{-1}\right) =$$

$$= z_{eq} e^{j\varphi_{eq}} = R_{eq} + jX_{eq};$$

$$s = (\omega_e - \omega_r)/\omega_e .$$

Let F = 1. Then from (6) the slip of the IG can be given by

$$s = r_2\left(\sqrt{1-4a_0X_{lr}^2}-1\right)/\left(2a_0X_{lr}^2\right), \quad (8)$$

and from (7) the magnetizing reactance of the IG can be obtained as

$$X_m = X_{mb} = b_0\left(r_2^2 + X_{lr}^2 s^2\right)/\left(\left(b_1X_{lr}^2 - b_0X_{lr}\right)s^2 + b_1r_2^2\right), \quad (9)$$

where

$$a_0 = \frac{a_1R_m + \left(a_1^2 + a_2^2\right)}{\left(a_1^2 + a_2^2\right)R_m}; \quad a_1 = r_1 + \frac{X_{es}^2R_{eq}}{a_3};$$

$$a_2 = X_{ls} - \frac{R_{eq}^2X_{es}}{a_3} - \frac{X_{eq}X_{es}\left(X_{eq} - X_{es}\right)}{a_3};$$

$$a_3 = R_{eq}^2 + \left(X_{eq} - X_{es}\right)^2; \quad b_0 = a_1^2 + a_2^2; \quad b_1 = -a_2 .$$

The air gap voltage of the IG U_m can be determined from the $X_m = U_{mb}(X_{mb})$ curve obtained from the synchronous speed test at rated speed.

The rotor electrical speed, phase current, phase voltage and per-phase input admittance of the IG are computed using the following equations

$$\omega_r = (1-s)\omega_e ; \quad (10)$$

$$I_{ph} = U_mY_S ; \quad (11)$$

$$U_{ph} = -jI_{ph}X_{es}z_{eq}e^{j\varphi_{eq}}/\left(z_{eq}e^{j\varphi_{eq}} - jX_{es}\right); \quad (12)$$

$$y_1 = \left(r_1 + jX_{ls} + \left(Y_m + Y_R\right)^{-1}\right)^{-1} = 0 . \quad (13)$$

It should be noted that the EC of Fig. 2 allows us to analyze not all the operating modes of the HPSS of Fig. 1, but only those in which the condition ω_e = const or ω_r = const is valid.

The methodology for performance analysis of the IG driven by the HT of the master-HTGU and operating in the proposed system of Fig. 1 is outlined as follows.

At first, we will obtain the performance characteristics of the stand-alone IG.

1. Set up the power factor of the load $\cos\varphi_L$, a $k1\times1$ column vector of the impedance of the local load $\boldsymbol{Z_L}$ and a $h1\times1$ column vector of trial values of the total reactive impedance of the BCC and VSC1 $\boldsymbol{X_{es}^{ig}}$

$$\boldsymbol{Z_L} = \left(z_{k,h}\right)_{k1\times1}, \quad \boldsymbol{X_{es}^{ig}} = \left(x_{h,k}\right)_{h1\times1} . \quad (14)$$

2. Find the elements of the air gap voltage matrix using magnetization characteristic of the IG and (9), phase current and voltage matrixes according to (11), (12), slip and input admittance matrixes of the IG according to (8), (13) using all combinations of elements of $\boldsymbol{Z_L}$ and $\boldsymbol{X_{es}^{ig}}$ vectors

$$\boldsymbol{U_m^{ig}} = \left(um_{k,h}\right)_{k1\times h1}, \quad \boldsymbol{I_{ph}^{ig}} = \left(iph_{k,h}\right)_{k1\times h1},$$

$$\boldsymbol{U_{ph}^{ig}} = \left(uph_{k,h}\right)_{k1\times h1}, \quad \boldsymbol{SI^{ig}} = \left(s_{k,h}\right)_{k1\times h1}, \quad (15)$$

$$\boldsymbol{YI^{ig}} = \left(y1_{k,h}\right)_{k1\times h1}.$$

3. Set the phase voltage reference of the IG and in each row of the $\boldsymbol{U_m^{ig}}$ (k = const, h = var) array determine the number of the column corresponding to the minimum deviation of the actual voltage from the reference $U_g^* = \text{const}$. Save the found column numbers into a one-dimensional array. Further, from the matrices (15), we form $k1\times1$ column vectors of the air gap voltage $\boldsymbol{U_m^{ig,uc}}$, phase current $\boldsymbol{I_{ph}^{ig,uc}}$, phase voltage $\boldsymbol{U_{ph}^{ig,uc}}$, input admittance of the IG $\boldsymbol{YI^{ig,uc}}$, slip $\boldsymbol{SI^{ig,uc}}$, electrical angular speed of the rotor $\boldsymbol{W_r^{ig,co}}$ and the total reactive impedance of the BCC and VSC1 $\boldsymbol{X_{es}^{ig,uc}}$ ensuring the performance with the least voltage error for each load value .

4. From the $\boldsymbol{X_{es}^{ig,uc}}$ vector we find the reactive impedance of the BCC $X_{nl} = X_{es}^{ig,uc}[i1]$, where the index $i1$ corresponds to the element with maximum impedance of the local load array $Z_L[i1] = \max\left(z_{k,h}\right)_{k1\times1}$.

5. Find the elements of the per-phase reactance, the phase current and the apparent power of the VSC1 arrays $\boldsymbol{X_{VSC1}^{ig,uc}}$, $\boldsymbol{I_{VSC1}^{ig,uc}}$, $\boldsymbol{S_{VSC1}^{ig,uc}}$, the power factor array and efficiency array $\boldsymbol{PF_{IG}^{ig,uc}}$, $\boldsymbol{EF_{IG}^{ig,uc}}$ of the IG

$$X_{VSC1}^{ig,uc}[k] = \left(\frac{1}{X_{es}^{ig,uc}[k]} - \frac{1}{X_{nl}}\right)^{-1}; \quad (16)$$

$$I_{VSC1}^{ig,uc}[k] = \frac{U_{ph}^{ig,uc}[k]}{X_{VSC1}^{ig,uc}[k]}; \quad (17)$$

$$S_{VSC1}^{ig,uc}[k] = Q_{VSC1}^{ig,uc}[k] = 3\frac{\left|U_{ph}^{ig,uc}[k]\right|^2}{X_{VSC1}^{ig,uc}[k]}; \quad (18)$$

$$PF_{IG}^{ig,uc}[k] = \frac{\mathrm{Re}\left(Y1^{ig,uc}[k]\right)}{\left|Y1^{ig,uc}[k]\right|}; \quad (19)$$

$$EF_{IG}^{ig,uc}[k] = \frac{P_L^{ig,uc}[k]}{P_L^{ig,uc}[k] + P_{Cu}^{ig,uc}[k] + P_{Fe}^{ig,uc}[k] + P_{Fr}^{ig,uc}[k]}, \quad (20)$$

where $P_{Cu}^{ig,uc}[k] = P_{Cu1}^{ig,uc}[k] + P_{Cu2}^{ig,uc}[k]$; $\boldsymbol{P_L^{ig,uc}}$, $\boldsymbol{P_{Cu1}^{ig,uc}}$, $\boldsymbol{P_{Cu2}^{ig,uc}}$, $\boldsymbol{P_{Fe}^{ig,uc}}$, $\boldsymbol{P_{Fr}^{ig,uc}}$ are column vectors of real power of the load, stator copper losses, rotor copper losses, core losses and friction losses;

$$P_L^{ig,uc}[k] = 3\frac{\left(U_{ph}^{ig,uc}[k]\right)^2}{\left|Z_L[k]\right|}\cos\varphi_L ;$$

$$P_{Cu1}^{ig,uc}[k] = 3\left(I_{ph}^{ig,uc}[k]\right)^2 r_1 ;$$

$$P_{Cu2}^{ig,uc}[k] = 3\left|\frac{U_m^{ig,uc}[k]}{jX_{lr} + r_2/S1^{ig,uc}[k]}\right|^2 r_2 ;$$

$$P_{Fe}^{ig,uc}[k] = 3R_m\left|\frac{U_m^{ig,uc}[k]}{R_m}\right|^2; \quad P_{Fr}^{ig,uc}[k] = k_{Fr}FP_{gN} ;$$

k_{Fr} – friction coefficient; P_{gN} – nominal power of the IG.

Next, we will use the principle of superposition and compute the performance characteristics of the IG operating in the system of Fig. 1 by superposition of power curves of other elements and power curves of the stand-alone IG. The principle and method of superposition are applied to determine currents and voltages in linear circuits and sometimes for obtaining performance characteristics of AC systems with parallel power sources [19]. For the off-grid mode of the HPSS of Fig. 1 when the Fig. 2 EC is used, the relation between the active power of the IG and the active power of the load due to the power transmission losses neglected is linear. Other elements such as WT, RDL and ESS are represented in the EC by linear resistances. Therefore, the principle of superposition can be applied in this case.

Assume the ESS is charged and the output power of the WT P_{WG} is constant. First, let's add WT and RDL to the stand-alone HTGU with IG, assuming that ESS has no influence on the control of the RDL. Accordingly to (4) and (5) if $\omega^*_{\min} < \omega_e < \omega^*_{\max}$, this is possible under the condition that the ESS is not used or the ESS controller limits the current value of the IG when $\Delta P^*_{EL} \ge 0$, i.e. when there is no excess of active power in the system. The said condition in the system of Fig. 1 will be satisfied if the charged ESS will not be discharged in the no load mode of the IG, that is, practically always in steady state. Taking into account the above assumptions, in the absence of a steady state power error, the power of the RDL will be given by

$$P_{DL}[k] = P^*_{EX} + \Delta P^*_{DL}[k], \quad (21)$$

where

$$\Delta P^*_{DL}[k] = \begin{cases} 0, P_{WG} - P^{ig,uc}_L[k] < P^*_{EX} \\ P_{WG} - P^{ig,uc}_L[k] - P^*_{EX}, P_{WG} - P^{ig,uc}_L[k] \ge P^*_{EX} \end{cases}.$$

6. Determine the active power of the IG when the RDL and WT are connected (ON) and the ESS is disconnected (OFF) from the HPSS

$$P^{WD}_{IG}[k] = P^{ig,uc}_L[k] + P_{DL}[k] - P_{WG}. \quad (22)$$

7. The phase current of the IG when the RDL and WT are ON and the ESS is OFF can be obtained by interpolation of the relation between values of elements of the array of the real power of the load $\boldsymbol{P^{ig,uc}_L}$ and the array of the phase current values $\boldsymbol{I^{ig,uc}_{ph}}$ of the stand-alone IG

$$I^{WD}_{ph}[k] = \text{inter}\left(\boldsymbol{P^{ig,uc}_L}, \boldsymbol{I^{ig,uc}_{ph}}, P^{WD}_{IG}[k]\right). \quad (23)$$

The next step is to add the ESS to the system and determine the following values.

8. The ESS power provided there is no steady state power error

$$P_{ES}[k] = \begin{cases} 0, I^{WD}_{ph}[k] < I^*_{g.\max}; \\ P^{WD}_{IG}[k] - P^*_{g.\max}, I^{WD}_{ph}[k] \ge I^*_{g.\max}, \end{cases} \quad (24)$$

where $P^*_{g.\max} = \text{inter}\left(\boldsymbol{I^{WD}_{ph}}, \boldsymbol{P^{WD}_{IG}}, I^*_{g.\max}\right)$ is real power of the IG with ESS is OFF and $I_{ph} = I^*_{g.\max}$.

9. Real power of the IG when RDL ,WT and ESS are ON

$$P^{WDE}_{IG}[k] = P^{ig,uc}_L[k] + P_{DL}[k] - P_{WG} - P_{ES}[k]. \quad (25)$$

10. Equivalent impedance of the per-phase load of the IG when RDL ,WT and ESS are ON

$$Z^{WDE}_L[k] = \left(\frac{1}{Z_L[k]} + \frac{P_{DL}[k] - P_{WG} - P_{ES}[k]}{3\left(U^*_g\right)^2} \right)^{-1} = \quad (26)$$

$$= \left(1/Z_L[k] + 1/R^{WDE}_{VSC1}[k]\right)^{-1},$$

where $\boldsymbol{R^{WDE}_{VSC1}}$ is the column vector of the per-phase equivalent resistances of the VSC1

11. Repeat steps 2–5 using the $\boldsymbol{Z^{WDE}_L}$ array instead of the $\boldsymbol{Z_L}$ array. As a result, we get new $k1\times1$ air gap voltage array $\boldsymbol{U^{WDE}_m}$, phase current array $\boldsymbol{I^{WDE}_{ph}}$, phase voltage array $\boldsymbol{U^{WDE}_{ph}}$, input admittance array of the IG $\boldsymbol{Y1^{WDE}}$, slip array $\boldsymbol{S1^{WDE}}$, electrical angular speed array of the rotor $\boldsymbol{W^{WDE}_r}$, total per phase reactance of the BCC and VSC1 array $\boldsymbol{X^{WDE}_{es}}$, and reactance array of the VSC1 when RDL ,WT and ESS are ON $\boldsymbol{X^{WDE}_{VSC1}}$.

Compute the elements of the following arrays for the «full» HPSS (RDL ,WT and ESS are ON).

12. The per phase impedance array and phase current array of the VSC1

$$Z^{WDE}_{VSC1}[k] = -jX^{WDE}_{VSC1}[k] + R^{WDE}_{VSC1}[k]; \quad (27)$$

$$I^{WDE}_{VSC1}[k] = U^{WDE}_{ph}[k] / Z^{WDE}_{VSC1}[k]. \quad (28)$$

13. The real power array, reactive power array and apparent (total) power array of the VSC1

$$P^{WDE}_{VSC1}[k] = -3\left|U^{WDE}_{ph}[k]\right|^2 / R^{WDE}_{VSC1}[k]; \quad (29)$$

$$Q^{WDE}_{VSC1}[k] = 3\left|U^{WDE}_{ph}[k]\right|^2 / X^{WDE}_{VSC1}[k]; \quad (30)$$

$$S^{WDE}_{VSC1}[k] = \sqrt{\left(P^{WDE}_{VSC1}[k]\right)^2 + \left(Q^{WDE}_{VSC1}[k]\right)^2}. \quad (31)$$

14. The power factor array $\boldsymbol{PF^{WDE}_{IG}}$ and efficiency array $\boldsymbol{EF^{WDE}_{IG}}$ of the IG are determined from (19), (20) using $\boldsymbol{Y1^{WDE}}$, $\boldsymbol{I^{WDE}_{ph}}$, $\boldsymbol{U^{WDE}_{ph}}$, $\boldsymbol{U^{WDE}_m}$, $\boldsymbol{S1^{WDE}}$ arrays instead of $\boldsymbol{Y1^{ig,uc}}$, $\boldsymbol{I^{ig,uc}_{ph}}$, $\boldsymbol{U^{ig,uc}_{ph}}$, $\boldsymbol{U^{ig,uc}_m}$, $\boldsymbol{S1^{ig,uc}}$ arrays.

Results. The performance analysis of the 250 kW IG operating both in the stand-alone HTGU and in the HTGU of the HPSS of Fig. 1 was carried out using the explained above methodology with values of the power factor of the load 1 (Fig. 3) and 0.9 (Fig. 4). It was set $P^*_{EX} = 0.1$ p.u., P_{WG} = 0.3 p.u., $U^*_g = 1$ p.u. and $I^*_{g.\max} = 1$ p.u.

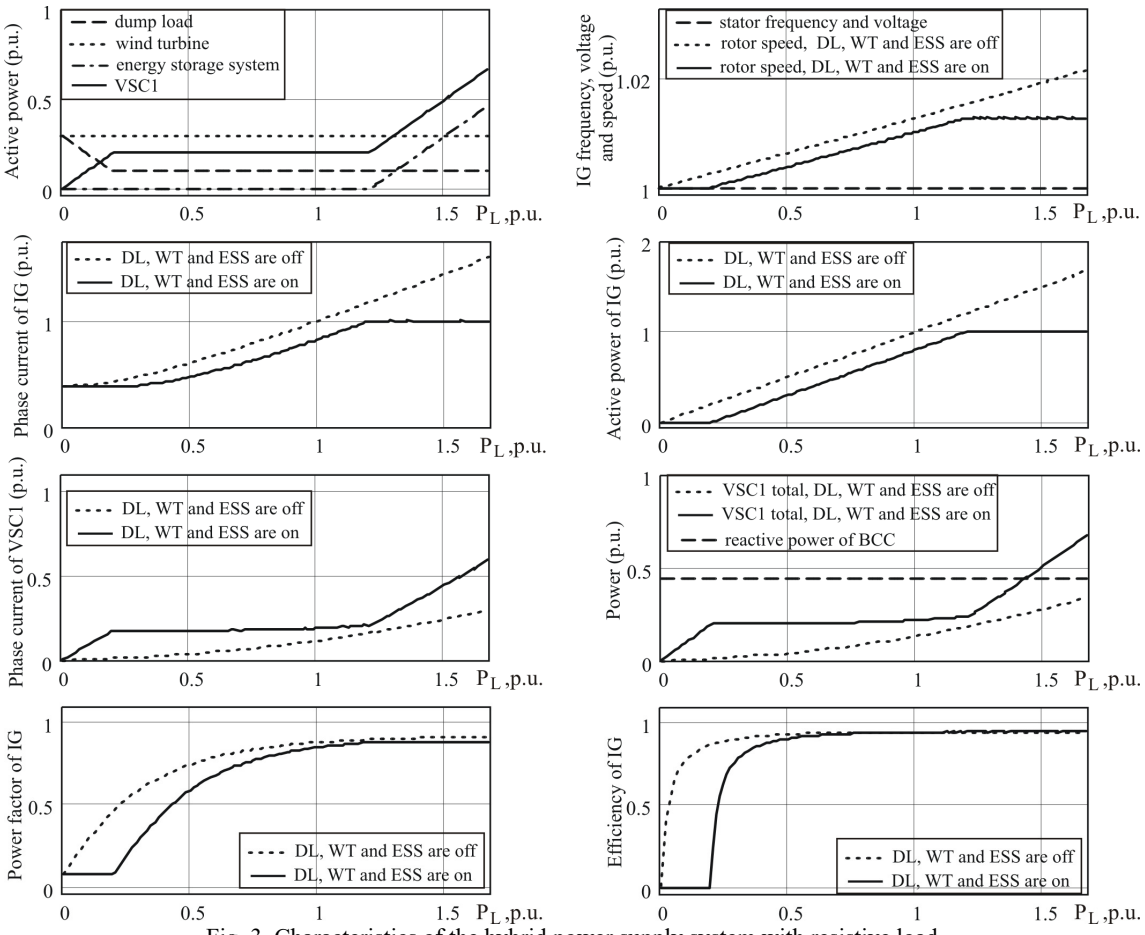

Fig. 3. Characteristics of the hybrid power supply system with resistive load

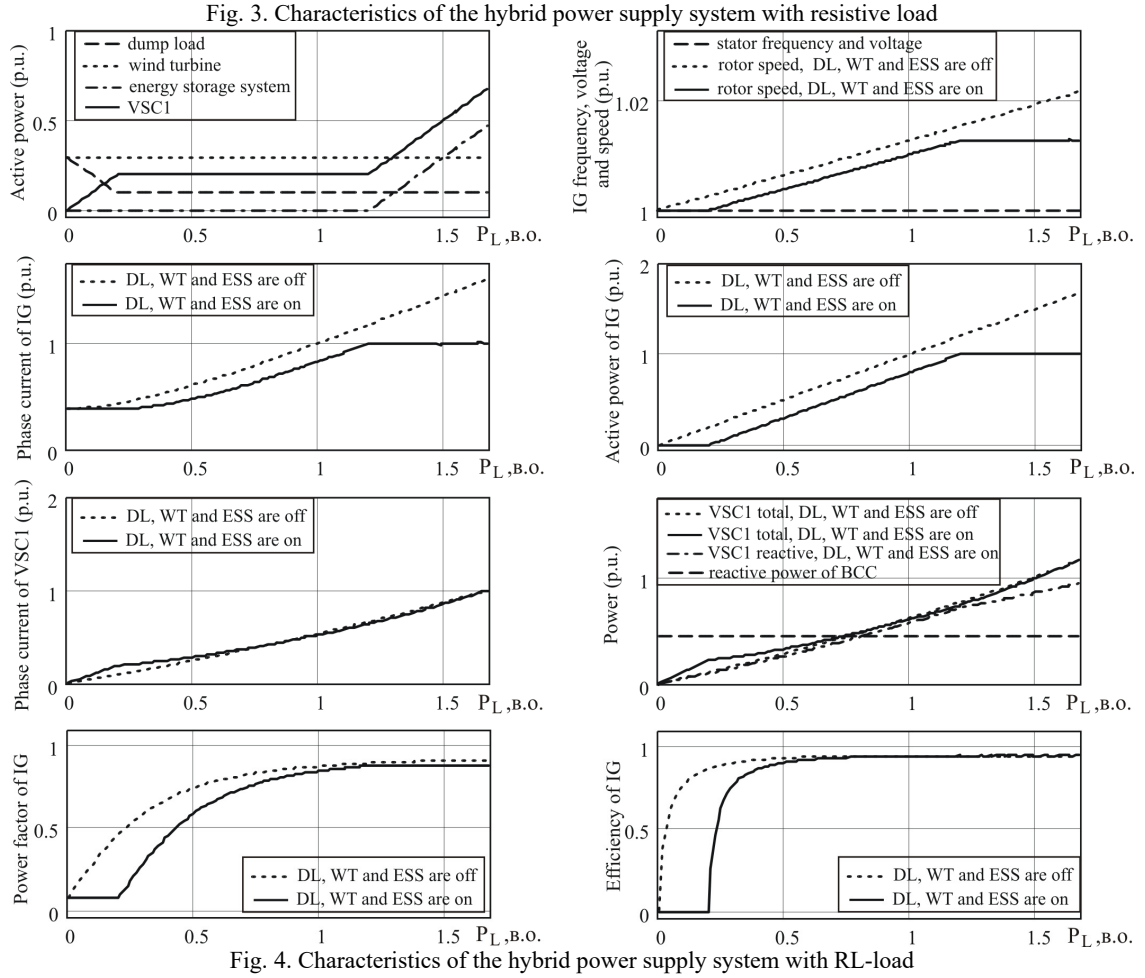

Fig. 4. Characteristics of the hybrid power supply system with RL-load

As can be seen from Fig. 3 and Fig. 4, the characteristics of the IG under resistive and RL local load are much similar. Since $P_{WG} > P_{EX}^{*}$, then during operation of the HTGU with IG in the HPSS running on low (0…0.2 p.u.) load, there is excess of active power generated in the system, which is consumed by the RDL, the real power of the IG G1 is zero, and the electrical rotor speed is near to the synchronous speed. When the IG current value reaches 1 p.u., the linear increasing in power of the ESS is observed and due to this the current and active power values of the IG stay at the nominal level. The power factor and efficiency values of the IG remain unchanged while there is excess of active power generated. The rotor speed within the load power range corresponding to 1 p.u. IG current value is constant as well.

Differences between Fig. 3 and Fig. 4 refer only to the characteristics of the VSC1 converter. Since the VSC1 converter for voltage control of the IG load, in addition to the compensation of the reactive power of the IG, must compensate under RL local load its reactive power, accordingly the values of the phase current and apparent power of the VSC1 are much greater than while supplying the resistive load. As can be seen from Fig. 3 and Fig. 4, when the value of the real power component of the load P_L is 1 p.u. and the IG is operating in the stand-alone HTGU, then the ratio of currents and apparent powers of the VSC1 obtained under resistive and RL-load is 1:4.7. When the IG is operating in the HPSS of Fig. 1, this ratio is 1:2.8.

At the same time, the values of the current and apparent power of the VSC1 during the operation of the IG in the «full» HPSS running under P_L = 1 p.u. load power when the load is resistive are 1.7 greater than during stand-alone operation of the HTGU and approximate to each other under RL-load. The power factor of the IG operating in the stand-alone HTGU in the entire load range, except for no load point, is greater than the power factor of the IG operating in the HPSS of Fig. 1. The maximum efficiency value of the IG operating in the stand-alone HTGU and in the HPSS of Fig. 1 was 0.947, and the maximum power factor value of the IG was 0.91 and 0.88 in stand-alone mode and for in system operation, respectively. These values correlate well with specifications of serial induction machines.

Simulation parameters and characteristics.

IG G1. Rated power / voltage / frequency / poles / (connection) – 250 kW / 400 V / 50 Hz / 4 / (Y); resistance of the stator / rotor winding, mΩ – 7.7 / 7.7; stator / rotor leakage reactance, mΩ – 33 / 33; core loss resistance, Ω – 42.3; friction coefficient, N·m·s/rad – 0.015. The magnetization characteristic of the IG is given in the Table 1.

Table 1

Magnetization characteristic of the IG G1

Phase current, A	20	27	54	105	141	191	290	421	592	836
Phase voltage, V	99	110	154	201	221	243	265	287	310	331

WT, RDL, ESS, VSC1, load, BCC, inductors. The output power of the WT is 0.3 p.u.; P_{EX}^{*} = 0.1 p.u.; the ESS is charged and limits the current value of the generator to the 1 p.u. value; losses in the VSC1 converter and inductors are neglected; the local load is symmetrical resistive or RL with a power factor of 0.9; the per phase capacity of the BCC is 2.2 mF.

Base quantities of power, voltage, current, speed and frequency for Fig. 3, 4 data. 250 kW = 1 p.u. of power; 230 V = 1 p.u. of voltage; 418 A = 1 p.u. of current; 1500 rpm = 1 p.u. of rotational speed; 50 Hz = 1 p.u. of frequency.

Conclusions. The methodology for steady state performance analysis of the induction generator driven by a hydraulic turbine of the master hydropower turbine equipped generating unit and operating in «constant voltage – constant frequency» mode in parallel through an electronic AC/DC power converter with sources and consumers of active power in the hydro-wind-battery hybrid power supply system supplying a three phase load has been developed.

Known methodologies for steady state performance analysis of isolated hybrid power systems using induction generators and regulated static energy converters are dynamic model based and thus are quite complex in use and modification. In contrast to known methodologies of steady state performance analysis of self-excited induction generator and parallel operated induction generators, superposition method and interpolation of characteristics are used to take into account additional power sources and consumers with preset control algorithms in the developed methodology. With the developed methodology it is possible to calculate performance of the system under study for an arbitrary output voltage reference thanks to the parametric analysis of this system provided in the methodology.

Approbation of the developed methodology was carried out on the isolated power system using a 250 kW induction generator. The obtained characteristics of the induction generator operating in the system differ from the characteristics of the stand-alone hydropower turbine equipped generating unit and depend on the characteristics and control algorithms of the additional sources and consumers of active power of the system. It was shown that, when the system supplied a local load with nominal real power component, the reduction of the power factor of the load from 1 to 0.9 led to an increase in the values of the apparent power and input currents of the AC/DC converter by 4.7 times in the stand-alone mode of operation of the hydropower turbine equipped generating unit and 2.8 times when the unit operated in the system. Due to this a significant increase in the installed capacity of the AC/DC converter both for stand-alone operation mode of the hydropower turbine equipped generating unit, and for its operation in the system supplying RL-load, is required in contrast to operation with resistive load. The obtained values of the maximum power factor and efficiency of the induction generator correlate well with the technical characteristics of serial asynchronous machines.

Further improvement and development of the outlined methodology can be carried out thanks to a more accurate calculation of losses and consideration of new modes of operation and circuit solutions of hybrid power systems.

Conflict of interest. The authors declare that they do not have conflicts of interest.

REFERENCES

1. Vita V., Alimardan T., Ekonomou L. The Impact of Distributed Generation in the Distribution Networks' Voltage Profile and Energy Losses. *IEEE European Modelling Symposium (EMS)*, Madrid, Spain, 2015, pp. 260-265. doi: https://doi.org/10.1109/EMS.2015.46.

2. Zharkin A., Novskyi V., Palachov S., Pazieiev A., Malakhatka D. Means of Electromagnetic Compatibility Providing In Local Electricity Networks Under Distributed Generation Development. *2020 IEEE 4th International Conference on Intelligent Energy and Power Systems (IEPS)*, Istanbul, Turkey, 2020, pp. 57-62. doi: https://doi.org/10.1109/IEPS51250.2020.9263199.

3. Tebbakh N., Labed D., Labed M.A. Optimal size and location of distributed generations in distribution networks using bald eagle search algorithm. *Electrical Engineering & Electromechanics*, 2022, no. 6, pp. 75-80. doi: https://doi.org/10.20998/2074-272X.2022.6.11.

4. Shavelkin A.A., Gerlici J., Shvedchykova I.O., Kravchenko K., Kruhliak H.V. Management of power consumption in a photovoltaic system with a storage battery connected to the network with multi-zone electricity pricing to supply the local facility own needs. *Electrical Engineering & Electromechanics*, 2021, no. 2, pp. 36-42. doi: https://doi.org/10.20998/2074-272X.2021.2.06.

5. Bhutto D.K., Ansari J.A., Bukhari S.S.H., Chachar F.A. Wind Energy Conversion Systems (WECS) Generators: a Review. *2nd International Conference on Computing, Mathematics and Engineering Technologies (iCoMET)*, Sukkur, Pakistan, 2019, pp. 1-6. doi: https://doi.org/10.1109/ICOMET.2019.8673429.

6. Mazurenko L.I., Kotsiuruba A.V., Dzhura O.V., Shykhnenko M.O. Voltage and Power Regulation of an Induction Generator-Based Hydroelectric Power Plant. *IEEE International Conference on Modern Electrical and Energy Systems (MEES)*, Kremenchuk, Ukraine, 21-24 September 2021, pp. 1-6. doi: https://doi.org/10.1109/MEES52427.2021.9598549.

7. Boukadoum A., Bouguerne A., Bahi T. Direct power control using space vector modulation strategy control for wind energy conversion system using three-phase matrix converter. *Electrical Engineering & Electromechanics*, 2023, no. 3, pp. 40-46. doi: https://doi.org/10.20998/2074-272X.2023.3.06.

8. Singh B., Murthy S.S., Gupta S. Analysis and design of electronic load controller for self-excited induction Generators. *IEEE Transactions on Energy Conversion*, 2006, vol. 21, no. 1, pp. 285-293. doi: https://doi.org/10.1109/TEC.2005.847950.

9. Alghuwainem S.M. Steady-state analysis of self-excited induction generator using real and reactive power balances. *IEEE 27th Canadian Conference on Electrical and Computer Engineering (CCECE)*, Toronto, ON, Canada, 2014, pp. 1-4. doi: https://doi.org/10.1109/CCECE.2014.6900964.

10. Wang L., Yang Y.-F., Kuo S.-C. Analysis of grid-connected induction generators under three-phase balanced conditions. *IEEE Power Engineering Society Winter Meeting. Conference Proceedings (Cat. No.02CH37309)*, New York, NY, USA, 2002, vol. 1, pp. 413-417. doi: https://doi.org/10.1109/PESW.2002.985033.

11. Popovych O., Golovan I., Shevchuk S., Listovshchyk L. Means of Complex Design of the Electromechanical System of the Gravity Energy Storage of the WindPower Plant. *2022 IEEE 8th International Conference on Energy Smart Systems (ESS)*, Kyiv, Ukraine, 2022, pp. 149-152. doi: https://doi.org/10.1109/ESS57819.2022.9969243.

12. Vanfretti L., Li W., Bogodorova T., Panciatici P. Unambiguous power system dynamic modeling and simulation using modelica tools. *2013 IEEE Power & Energy Society General Meeting*, Vancouver, BC, Canada, 2013, pp. 1-5. doi: https://doi.org/10.1109/PESMG.2013.6672476.

13. Hernández-Mayoral E., Dueñas-Reyes E., Iracheta-Cortez R., Campos-Mercado E., Torres-García V., Uriza-Gosebruch R. Modeling and Validation of the Switching Techniques Applied to Back-to-Back Power Converter Connected to a DFIG-Based Wind Turbine for Harmonic Analysis. *Electronics*, 2021, vol. 10, no. 23, art. no. 3046. doi: https://doi.org/10.3390/electronics10233046.

14. Louze L., Abdessemad O., Nemmour A., Khezzar A. An Effective Control of an Isolated Induction Generator Supplying DC Load for Wind Power Converting Applications. *Electrical Engineering & Electromechanics*, 2020, no. 3, pp. 65-69. doi: https://doi.org/10.20998/2074-272X.2020.3.10.

15. Sobczyński D., Pawłowski P. Energy storage systems for renewable energy sources. *2021 Selected Issues of Electrical Engineering and Electronics (WZEE),* Rzeszow, Poland, 2021, pp. 1-4, doi: https://doi.org/10.1109/WZEE54157.2021.9576964.

16. Yang P., Nehorai A. Joint Optimization of Hybrid Energy Storage and Generation Capacity With Renewable Energy. *IEEE Transactions on Smart Grid*, 2014, vol. 5, no. 4, pp. 1566-1574. doi: https://doi.org/10.1109/TSG.2014.2313724.

17. Mazurenko L.I., Dzhura O.V., Kotsiuruba A.V., Shykhnenko M.O. A Wind-Hydro Power System Using a Back-to-Back PWM Converter and Parallel Operated Induction Generators. *IEEE Problems of Automated Electrodrive. Theory and Practice (PAEP)*, Kremenchuk, Ukraine, September 21-25, 2020, pp. 1-5. doi: https://doi.org/10.1109/PAEP49887.2020.9240777.

18. Xie J., Zheng Y., Pan X., Zheng Y., Zhang L., Zhan Y. A Short-Term Optimal Scheduling Model for Wind-Solar-Hydro Hybrid Generation System With Cascade Hydropower Considering Regulation Reserve and Spinning Reserve Requirements. *IEEE Access*, 2021, vol. 9, pp. 10765-10777. doi: https://doi.org/10.1109/ACCESS.2021.3049280.

19. Engler A., Hardt C., Strauss P., Vandenbergh M. Parallel Operation of Generators for Stand-Alone Single-Phase Hybrid Systems-First Implementation of a new control Technology. 2001. Available at: https://www.researchgate.net/publication/228944407_Parallel_Operation_of_Generators_for_Stand-Alone_Single-Phase_Hybrid_Systems-First_Implementation_of_a_new_control_Technology (accessed 31.03.2023).

Received 30.08.2023
Accepted 02.10.2023
Published 02.03.2024

L.I. Mazurenko[1], *Doctor of Technical Science, Professor,*
O.V. Dzhura[1], *PhD, Senior Research Scientist,*
M.O. Shykhnenko[1], *PhD, Research Scientist,*
[1] Institute of Electrodynamics National Academy of Sciences of Ukraine,
56, Prospect Beresteiskyi, Kyiv-57, 03057, Ukraine,
e-mail: mlins@ied.org.ua;
suoma1715@gmail.com (Corresponding Author);
s.maxim@email.ua

How to cite this article:
Mazurenko L.I., Dzhura O.V., Shykhnenko M.O. Steady-state analysis of a hybrid power supply system using an induction generator with a shunt AC/DC converter. *Electrical Engineering & Electromechanics*, 2024, no. 2, pp. 67-74. doi: https://doi.org/10.20998/2074-272X.2024.2.10